International Journal of Biological Macromolecules 120 (2018) 449–459

Contents lists available at ScienceDirect

International Journal of Biological Macromolecules

journal homepage: http://www.elsevier.com/locate/ijbiomac

Culled banana resistant starch-soy protein isolate conjugate based emulsion enriched with astaxanthin to enhance its stability

Smriti Shrestha, Muhammad Bilal Sadiq, Anil Kumar Anal *

Food Engineering and Bioprocess Technology, Department of Food, Agriculture and Bioresources, Asian Institute of Technology, Pathum Thani, Thailand

ARTICLE INFO

Article history:
Received 4 July 2018
Received in revised form 6 August 2018
Accepted 13 August 2018
Available online 15 August 2018

Keywords:
Resistant starch
Astaxanthin enriched emulsion
Biofortification
In vitro digestion
Thermal stability

ABSTRACT

The conjugates of biomacromolecules such as proteins and polysaccharides have potential to stabilize the emulsion system and encapsulate valuable bioactive compounds for biofortification in food systems. In this study, native banana starch (NBS) was isolated from green culled banana and modified into resistant starch (type III) by lintnerization followed by autoclaving-cooling process, resulting in lintnerized-autoclaved banana starch (LABS). Soy protein isolate (SPI) was used for developing the polysaccharide-protein conjugates *i.e.* LABS-SPI conjugate and used as wall material to stabilize the oil-in-water emulsion system. LABS-SPI conjugate emulsions were subjected to *in vitro* digestion model and oxidative stability evaluation. Furthermore, the emulsion system was enriched with astaxanthin and evaluated for its stability. The chemical finger printing of LABS-SPI conjugates showed stretching in immine and enaminol group of Schiff's bases, the C—N stretching of Amadori product. During *in vitro* digestion LABS-SPI conjugate emulsion showed that the presence of resistant starch had an influence on the droplet digestion process and significantly ($p < 0.05$) lower free fatty acid release compared to emulsions stabilized by SPI alone. LABS-SPI conjugate emulsion system demonstrated higher stability of astaxanthin at storage temperatures (6, 20 and 37 °C), and can be used for biofortification of food and pharmaceutical formulations.

1. Introduction

The emulsion system becomes an essential approach to encapsulate the bioactive materials for biofortification and to enhance their stability in functional food formulations, their targeted delivery and controlled release to enhance the bioavailability [1,2]. Emulsions are thermodynamically unstable and tend to collapse due to different physicochemical processes. However, kinetically stable emulsions are generally formulated using intense mechanical forces along with various emulsifiers [3].

Proteins are commonly used natural emulsifiers to stabilize the oil-in-water emulsions. Due to amphiphilic nature, proteins are adsorbed at the oil-water interface and exhibit electrostatic and/or steric repulsion that prevents droplet aggregation and coalescence [4]. However, in presence of organic solvent, high ionic strength or elevated temperature, proteins tend to lose emulsifying property that restricts their broad range of industrial applications [5]. On the other hand, polysaccharides with hydrophilic nature act as stabilizer and thickening agent at a wide range of pH and ionic strength but exhibit lower interfacial property due to lack of lipophilic moieties and granular structures [6]. Protein-polysaccharide conjugates, therefore, combine the protein emulsification properties and polysaccharide stabilizing effects in such a way that hydrophobic protein adsorbs to oil droplet surface and hydrophilic polysaccharide adsorbs to the aqueous phase medium resulting in improved steric stabilization. The conjugates formed by covalent interactions of protein and polysaccharides showed stability to changes in pH, ionic strength and temperature with improved emulsifying properties, solubility and heat stability [7].

Resistant starch (RS) is the sum of starch and products of starch degradation, which is not absorbed in the small intestine, but it is utilized as a substrate by probiotics in the large intestine and produces short chain fatty acids (SCFA) [8]. Globally, banana is one of the top ten crops in terms of yield and area of production in tropical and subtropical regions. However, about 20% of the total banana harvest is rejected due to under size or presence of damage spot on fruits, commonly known as culled bananas, which leads to environmental pollution and further economic loss [9]. As raw banana is generally rich in starch content (61.3 to 76.5% w/w), culled bananas have the potential for starch production at the lower cost compared to conventional sources such as wheat, corn and potato [10]. Resistant starch from green banana has been conjugated with proteins from different sources, including plant based protein (soy-protein isolate) [11], dairy proteins [12] and egg proteins [4] to stabilize the oil-in-water emulsion systems. However, the ability of resistant starch- protein conjugate based emulsion system has not been explored for encapsulation of bioactive compounds.

* Corresponding author at: Department of Food Agriculture and Bioresources, Asian Institute of Technology, Pathum Thani, 12120, Thailand.
E-mail address: anilkumar@ait.asia (A.K. Anal).

https://doi.org/10.1016/j.ijbiomac.2018.08.066
0141-8130/

Astaxanthin, a deep red colored carotenoid from green microalgae, *Haematococccus pluvialis* [13] presents a great deal of interest due to prevention of lipid peroxidation, antioxidant potential and impartation of coloration [14,15]. However, due to non-polar, unsaturated and conjugated structure, it is highly susceptible to degradation by exposure to light, high temperature and oxygen [16]. Different preservation techniques (structural modification, molecular inclusion and encapsulation) have been implemented to improve the stability and bioavailability of astaxanthin [17]. The aim of this study was to develop and characterize the culled banana resistant starch-soy protein isolate (CBRS-SPI) conjugate based emulsion and its application to enhance the stability of bioactive compounds. In this study, astaxanthin oleoresin extracted from microalgae, *Hematococcus pluvialis* was used as model compound. To our knowledge, none of the study has still been reported using culled banana resistant starch III and soy-protein isolate conjugate for developing the emulsion systems to encapsulate such bioactive compounds. This study also signifies as using the bio-waste, culled banana pulp and soy protein isolates.

2. Materials and methods

2.1. Materials

Kluai Namwa (*Musa* ABB group), culled bananas were purchased from the local market (Talad Thai, Pathumthani, Thailand). Resistant starch assay kit, Megazyme was acquired from Megazyme International Ireland. *Haematococcus pluvialis* astaxanthin oleoresin (10 wt% astaxanthin) was obtained from Yunnan Alphy Biotech Co. Ltd., China. α-amylase (from porcine pancreas, Product# A3176, ≥5 units/mg solid), mucin (from porcine stomach), bile extract (porcine, Product# 8631), pepsin (from porcine gastric mucosa, Product# P7000, ≥250 U/mg solid) and pancreatin (from porcine pancreas, Product# 76190, amylase >100 U/mg) were obtained from Sigma-Aldrich (USA). All other chemicals and reagents used were of analytical grade.

2.2. Preparation of culled banana resistant starch

Culled banana starch was isolated by alkaline extraction following the method of Nasrin and Anal [11] with slight modifications at the Bioprocess Technology Laboratory, Asian Institute of Technology, Thailand. The culled banana pulp was macerated in a blender (SHARP, EM-ICE-011661) with 0.05% NaOH solution (1:2 w/v) and steeped for 2 h followed by adding distilled water to the slurry (5:1 v/v). The slurry was sieved consecutively through 60, 100 and 200 mesh sieves (Endecotts Ltd., London, England). The starch sediment from the final filtrate (200 mesh sieve) was washed with distilled water, dried in oven (40 °C for 12 h) and named as native banana starch (NBS). For lintnerization process, the suspension of NBS in 2 N HCl solution (1:1.5 w/v) was further incubated at 40 °C for 3 h. The pH of the resultant mixture was adjusted to 6.5 with 10% (w/v) NaOH, followed by vacuum filtration and finally dried in an oven (40 °C for 12 h) to obtain the lintnerized banana starch (LBS). NBS and LBS were dispersed in distilled water (1:10 w/v) separately and gelatinized by heating at 85 °C for 30 min. The pre-gelatinized NBS and LBS were autoclaved at 135 °C for 30 min followed by cooling at 4 °C for 24 h to obtained resistant starch type III (retrograded starch). The autoclaving and cooling processes were repeated three times for each starch sample. The starch samples were finally lyophilized at −55 °C for 24 h in a freeze-dryer (Scanvac Coolsafe 55-4, Labogene, Lynge, Denmark), resulting in two types of resistant starches; native-autoclaved banana starch (NABS) and lintnerized autoclaved banana starch (LABS).

2.3. Chemical composition of culled banana starch

Resistant starch (RS) and non-resistant starch (NRS) contents of the native and treated banana starches were determined by Megazyme assay kit (Megazyme International Ltd., Ireland) following the manufacturer instructions. Amylose content of starch was determined following the iodine calorimetry method [18]. Mixture of starch (100 mg), ethanol (95%, v/v, 1 mL) and 1 N NaOH (10 mL) was heated at 100 °C for 10 min. The volume of the mixture was adjusted to 100 mL with distilled water. The aliquot (2.5 mL) from the mixture was mixed with 20 mL distilled water followed by dropping phenolphthalein (0.1% w/v). The HCl (0.1 N) was added drop-wise to the resultant mixture until the pink color disappeared. Iodine reagent (1 mL) was added to the mixture and the final volume was adjusted to 50 mL with distilled water. After 20 min incubation in dark, the absorbance was measured at 590 nm using UV-1800 spectrometer (Shimadzu, Kyoto, Japan). Iodine reagent (1 mL) diluted to final volume (50 mL) with distilled water was used as a blank. The calibration curve was prepared by using standard starch solutions containing 0, 20, 40, 60, 80 and 100% (w/v) amylose. Amylose content (percentage basis) in samples was determined with reference to the standard calibration curve.

2.4. Characterization of starch

The granular morphology of the starch samples was analyzed by scanning electron microscope (SEM) (JSM-6301F, JEOL Japan). The powdered starch samples were sprinkled on aluminum stubs with double sided adhesive tape, covered with a thin gold layer. After coating samples were examined at 20 kV acceleration potential and 1000× magnification.

Chemical fingerprinting of each starch sample was analyzed by Fourier transform infrared spectrometer (FTIR) (Perkin Elmer, USA). Samples were used directly for measurement of spectrum in the range of 500 to 4000 cm^{-1} wavenumbers.

2.5. Swelling power and solubility of the culled banana resistant starch

Swelling power and solubility of resistant starch samples were determined following Nasrin and Anal [11] with slight modifications. Resistant starch sample (1 g) was suspended in distilled water (50 mL) followed by incubation in shaking water bath (100 rpm) at 90 °C for 30 min. After cooling (25 °C), the suspension was centrifuged (Camloc Leicester, England) at 3000 rpm for 15 min. The weight of the wet sediment was measured to determine swelling power. On the other hand, the supernatant was dried at 105 °C for 4 h to analyze the solubility of starch. Swelling power and solubility were calculated by using Eqs. (1) and (2):

$$\text{Swelling power} = \frac{\text{weight of sediment}}{\text{weight of dry sample solids}} \quad (1)$$

$$\text{Solubility}\ (\%) = \frac{\text{weight of dry solids in supernatant}}{\text{weight of dry sample}} \text{x } 100 \quad (2)$$

2.6. Preparation and characterization of resistant starch-soy protein isolate conjugates

Resistant starch (LABS, selected based on chemical composition and functional properties) and soy protein isolate (SPI) were subjected to conjugation at three different ratios *i.e.* LABS: SPI ratio (1:1, 2:1 and 2:3, w/w), following the method of Nasrin and Anal [11] with slight modifications. Mixture of starch and protein was suspended in warm water at 60 °C to obtain an aqueous suspension of 10% (w/w) total solids and pH was maintained at 7.5 ± 0.2. The mixture was heated at 100 °C for 90 min followed by cooling (25 °C) and freeze-drying. Chemical fingerprinting of each LABS-SPI conjugate was analyzed by Fourier transform infrared spectrometer (FTIR) (Perkin Elmer, USA) in the range of 500 to 4000 cm^{-1} wavenumbers.

2.7. Preparation of emulsion

LABS-SPI conjugates were used as wall materials to formulate the oil-in-water based emulsions following the method of Jain and Anal [4] with slight modifications. Wall material was mixed with distilled water (60 °C) to obtain 5 and 10% (w/w) total solids under the stirring at 100 rpm (Velp Scientifica, Europe) for 6 h for complete hydration. Sunflower oil (oil phase) was added to the mixture to obtain 15% (w/w) total solid content of emulsion and pH was maintained initially at 7.5 ± 0.2. The coarse emulsion was prepared by blending the mixture (2000 rpm) for 2 min in a high performance commercial blender (OTTO, BE 127A, Thailand). The fine emulsion was further prepared by passing the coarse emulsion through high-pressure homogenizer (IKA Labor-pilot, 2000/4, Staufen, Germany) for three passages at 500 bars. The emulsion was stored in sterilized test tubes (4 ± 2 °C for 15 days) in dark conditions to evaluate the emulsion stability and creaming behavior. The emulsion, which exhibited better stability, was subjected to further analysis.

2.8. Emulsion stability and creaming index

Emulsion stability (ES) was determined following Zhao et al. [19] with slight modifications. ES was estimated by measuring the turbidity of the diluted emulsion (1:300 with 0.1%, w/v sodium dodecyl sulfate) at 500 nm by UV–vis spectrophotometer (Shimadzu, Kyoto, Japan) immediately after the emulsion was formed and after 3 h. ES (%) was calculated by using Eq. (3).

$$ES\ (\%) = \frac{\text{Absorbance at zero min}}{\text{Absrobance at 180 min}} \text{x } 100 \quad (3)$$

Creaming index (CI) of the emulsion was determined by measuring the change in height of the cream layer at the end of the storage period (15 days) and calculated by Eq. (4).

$$CI\ (\%) = \frac{\text{Height of the cream layer}}{\text{Initial height of the emulsion}} \text{x } 100 \quad (4)$$

2.9. Characterization of the stable emulsion

2.9.1. Emulsion oxidative stability

Oxidative stability of the emulsion was assessed in terms of peroxide value (PV) and thiobarbituric acid reactive substances (TBARS). Peroxide value (PV) was determined by the method as described by Kuhn & Cunhan [20] with slight modifications. Emulsion (0.3 mL) was added to 1.5 mL of isooctane/2-propanol (3:2 v/v), vortexed (3 times for 10 s) and allowed to stand for 30 min. The clear supernatant (200 μL) was added to 2.8 mL of chloroform/methanol (7:3, v/v) and vortexed for 4 s followed by the addition of 15 μL of ammonium thiocyanate (30%, w/v in water) with further vortexing for 4 s. The ferrous chloride solution (15 μL) was finally added to the sample, vortexed for 4 s followed by incubation at 25 °C for 5 min. The absorbance was measured at 500 nm against a blank by UV–vis spectrophotometer (Shimadzu, Kyoto, Japan). Hydroperoxide concentration was determined using a Fe^{+3} standard calibration curve and expressed as milliequivalents of peroxide per kilogram (meq/kg) of oil calculated by following Eq. (5).

$$\text{Peroxide Value } (PV) = \frac{\text{Absorbance of}(sample - blank) \times \text{slope of calibration curve}}{55.84 \times \text{mass of oil} \times 2} \quad (5)$$

TBARS value of emulsion was determined following the method of Zhao et al. [19] with slight modifications. The mixture containing emulsion (0.3 mL), deionized water (0.7 mL) and TBA reagent (2 mL) was incubated in water bath (100 °C) for 15 min. After cooling to 25 °C the mixture was subjected to centrifugation (5000 rpm) for 15 min (Camloc Leicester, England). The absorbance of the supernatant was measured at 532 nm by UV–vis spectrophotometer (Shimadzu, Kyoto, Japan) after 10 min of incubation at 25 °C. TBARS concentration was determined from a standard curve prepared with 1,1,3,3-tetrathoxypropane.

2.9.2. In vitro digestion of emulsion

The emulsion was passed through an *in vitro* digestion model that was comprised of simulated mouth, stomach and intestine phases following the method described by Jain and Anal [4] with slight modification.

Initial system: the initial emulsion system consisted of LABS-SPI conjugate stabilized emulsion. Emulsion (6 mL, pH 7.5) was placed into a glass beaker in a water bath at 37 °C.

Simulated mouth phase: Simulated saliva fluid (SSF) was prepared by adding 0.1594 g NaCl, 0.0202 g KCl, amylase (0.87% w/v) and 0.022 g mucin into phosphate buffer solution (PBS 10 mM, pH 7.0) to the final volume of 100 mL and pH was adjusted to 6.8. Initial emulsion (6 mL) was mixed with artificial saliva (6 mL) and incubated in water bath (37 °C for 5 min) with continuous shaking (100 rpm).

Simulated gastric phase: Simulated gastric fluid (SGF) was prepared by dissolving 0.32 wt% pepsin and 0.2 wt% NaCl in phosphate buffer (10 mM, pH 2.5). For *in vitro* gastric digestion, SGF (12 mL) was added to the emulsion resulting from simulated mouth phase (12 mL). The mixture (pH 2.5) was incubated in water bath (37 °C for 2 h) with continuous shaking (100 rpm).

Simulated intestinal phase: Simulated intestinal fluid (SIF) was prepared by adjusting pH 7.5 of the solution containing 39 mM K_2HPO_4, 150 mM NaCl and 30 mM $CaCl_2$. After mixing emulsion with SIF, bile extract (5 mg/mL) and pancreatin (1.6 mg/mL) were added. For *in vitro* intestinal digestion, SIF (24 mL) was added to the emulsion resulting from simulated gastric phase (24 mL). The mixture (pH 7) was incubated in water bath (37 °C for 2 h) with continuous shaking (100 rpm).

During *in vitro* digestion process, emulsion from each stage of digestion was diluted 50 times and analyzed for mean particles size, polydispersity index and zeta potential.

Zeta-potential of the emulsions were determined by using Zetasizer Nano ZS (ZEN 3600, Malvern Instrument Ltd., Malvern, Worcestershire, UK). Before analysis, samples were diluted to a droplet concentration of approximately 0.05 wt% using an appropriate buffer, such as the mouth phase sample was diluted using the simulated saliva fluid without mucin, gastric phase sample was diluted using the simulated gastric fluid without pepsin, and the other samples were diluted using the stock phosphate buffer (pH 7.0).

Droplet size and particle size distribution of the emulsion were determined by using a laser light scattering instrument (Mastersizer, 2000, Malvern Instruments Ltd., Malvern, Worcestershire, UK). The relative refractive index of the emulsion was 1.105, *i.e.*, the ratio of the refractive index of sun flower oil (1.47) to that of the aqueous medium (1.33). The mean particle size was reported as the volume-weighted mean diameter: d_{43}.

2.9.3. Determination of free fatty acid release

The degree of lipid digestion in SIF was determined in terms of free fatty acids (FFA's) by titration method [4]. Sample from intestinal phase (5 mL) was collected and mixed with acetone (10 mL) and phenolphthalein (1% w/v, 3 drops). The mixture was titrated with 0.1 N NaOH and the volume of NaOH required to reach the titration endpoint was noted. FFA released was determined by using following Eq. (6).

$$\%FFA = \frac{NaOH\ (Volume \times molarity) \times Molecular\ weight\ of\ oil}{Initial\ wt\ of\ oil\ x\ 2} \times 100 \quad (6)$$

2.10. Preparation of astaxanthin enriched emulsion

The oil phase was prepared by dispersing 1 g of astaxanthin oleoresin into 4 g of sunflower oil by magnetic stirring for 2 h and filtered through 0.45 μm membrane. Astaxanthin-enriched emulsion was prepared by using the parent emulsion composition.

2.11. Thermal stability of astaxanthin enriched emulsion

Astaxanthin enriched emulsions were stored under dark conditions at different temperatures (6 ± 1, 20 ± 1, 37 ± 1, 55 ± 1 and 70 ± 1 °C) for 15 days. Thermal stability of astaxanthin was evaluated by monitoring the change in color and the concentration of astaxanthin in the emulsions during storage. The color of the emulsion was measured according to Davidov-Pardo et al. [21] in terms of L*, a* b* color parameters of the CIELAB scale using a colorimeter (Hunter Lab Spectrocolorimeter, Model TC-P III A, Tokyo Denshoku Co., Ltd., Japan). The total color difference (ΔE) was calculated by using the following Eq. (7).

$$\Delta E = \sqrt{(L^* - L_i^*)^2 + (a^* - a_i^*)^2 + (b^* - b_i^*)^2} \quad (7)$$

where, L*, a*, b* are the color coordinates measured at time t, and L_i^*, a_i^* and b_i^* are the initial color coordinates measured initially.

The astaxanthin concentration in the emulsion was analyzed by following Liu et al. [22] with slight modifications. The emulsions (50 μl) were diluted to 100 times in DMSO (4.95 mL) and absorbance was measured at 478 nm by Uv-Vis spectrophotometer (Shimadzu, Kyoto, Japan) against the emulsion without astaxanthin diluted with DMSO as blank. Astaxanthin concentration was determined using standard calibration curve prepared from pure astaxanthin (98% purity) in DMSO in the range of 1 to 10 mg/L ($r^2 = 0.9976$). The first-order kinetic model (Eq. (8)) was used to estimate the astaxanthin degradation according to Niamnuy et al. [23].

$$\ln\left(\frac{C}{C_0}\right) = -kt \quad (8)$$

where, C_0 and C are the concentrations of astaxanthin at time 0 and any time t (day) respectively; t is the storage time (day); k is the temperature dependent astaxanthin degradation rate constant (day^{-1}) calculated as the negative slope of the plot of ln (C/C_0) *versus* t.

The effect of temperature on the degradation rate was measured using the Arrhenius relationship (Eq. (9))

$$\ln(k) = \ln(A) - \frac{E_a}{RT} \quad (9)$$

where, k is the astaxanthin degradation rate; A is a preexponential factor; E_a is activation energy; R is the universal gas constant (8.3145 J mol^{-1} K^{-1}); T is the absolute temperature in Kelvin. The plot of ln (k) *versus* 1/T was used to determine E_a which was calculated as the slope of the plot multiplied by the gas constant.

2.12. Statistical analysis

All the experiments were performed in triplicate and expressed as mean values ± standard deviation. Statistical analysis was conducted by using SPSS statistical software (SPSS, 23.0). ANOVA and Tukey's HSD test were carried out to determine the significant differences ($p < 0.05$) among the mean observations.

Table 1
Resistant starch, non-resistant starch and amylose content of banana starches.

Sample	RS II (%)	RS III (%)	NRS (%)	Amylose (%)
NBS	77.84 ± 3.14[a]	–	15.73 ± 0.33[a]	30.82 ± 0.11[a]
LBS	65.98 ± 2.16[b]	–	20.53 ± 0.11[b]	40.36 ± 0.2[b]
NABS	–	19.27 ± 0.25[c]	70.47 ± 0.75[c]	47.05 ± 0.15[c]
LABS	–	17.72 ± 1.49[c]	78.04 ± 0.17[d]	55.79 ± 0.04[d]

Values were expressed as means ± standard deviation (triplicate). Means with different superscripts (a–d) in the same column indicate the significant difference ($p < 0.05$). (NBS = native banana starch, LBS = lintnerized banana starch, NABS = native-autoclaved banana starch and LABS = lintnerized autoclaved banana starch).

3. Results and discussion

3.1. Chemical composition of starch

Table 1 presents the resistant starch (RS), non-resistant starch (NRS) and amylose contents of NBS, LBS, NABS and LABS. RS contents of NBS (77.84%) and LBS (65.98%) were recognized as RS II. Fig. 1 illustrates the smooth granular morphology of NBS and LBS without heat treatment. RS II content of NBS decreased significantly ($p < 0.05$) after lintnerization.

RS III was developed by two steps process *i.e.* autoclaving and cooling treatments. RS III contents of NABS (19.27%) and LABS (17.72%) were not significantly ($p < 0.05$) different but found higher in comparison to previous study (12.3% NABS and 13% LABS) reported by Nasrin and Anal, [11]. Reddy et al. [10] also reported that RS III content in enzymatically (Pullulanase) modified banana starch was about 25% (w/w).

During autoclaving, starch is gelatinized, and amylose chains leach out from the granules as random coils while in cooling treatment starch undergoes retrogradation and amylose chain recrystallize forming tightly packed double helices resistant to enzymatic hydrolysis [24]. During heat treatment, RS II of native starch converts to RS III due to re-crystallization of the short linear chains produced during retrogradation process [25].

Amylose content of the NBS (30.82%) was significantly increased after acid-hydrolysis (40.36% in LBS) and heat treatment (47.05% in NABS and 55.79% in LABS). Amylose content of banana starch was found to vary with the cultivars; 38.6–43.8% for six Kluai cultivar, 17–19.5% for Cavendish cultivar and 40.7% for Valery cultivar [26]. Aparicio-Saguilán et al. [27] reported significant increase in amylose content (37% to 45.5%) after lintnerization and heat treatment of native banana starch. Reddy et al. [10] reported an increase in amylose content from 23% to 40.46% after enzymatic hydrolysis followed by gelatinization and retrogradation of banana starch.

3.2. Characterization of resistant starch

3.2.1. Granular morphology

Fig. 1 illustrates the changes in granular morphology of the banana starch after acid hydrolysis and heat-treatment. NBS granules were both rod like and irregular oval shape with smooth surface indicating efficient starch isolation process [28]. Particle size diameter of NBS ranged from 12 to 40 μm. Nasrin et al. [29] reported that yellow plantain pulp starch presented elliptical smooth granules with 19–61 μm sizes. However, significant changes were observed in granular morphology of native starch after heat-treatment resulting in NABS and LABS with irregular shapes, resembling an amorphous mass of cohesive structure due to retrogradation of amylose chains leading to helical complex [10].

3.2.2. FT-IR spectrum of the starch

Fig. 2 illustrates the changes in chemical finger printing of native starch by FTIR spectrum after different treatments. The functional groups were assigned to their corresponding peaks (4000–500 cm^{-1}).

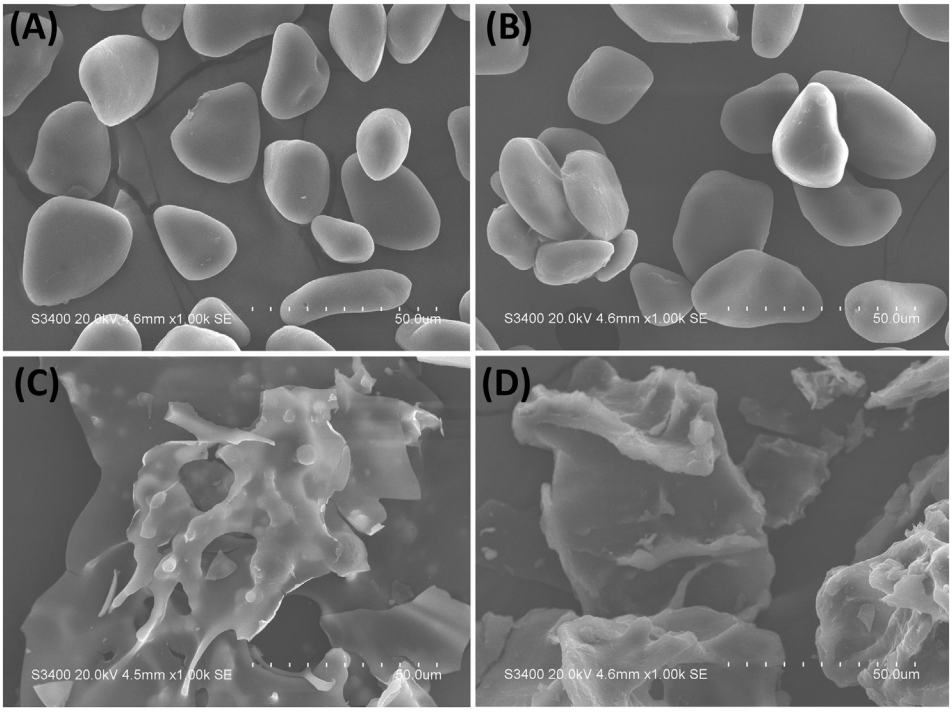

Fig. 1. Scanning electron microscopic image of starch (A) = NBS (native banana starch), (B) = LBS (lintnerized banana starch), (C) = NABS (native-autoclaved banana starch), (D) = LABS (lintnerized-autoclaved banana starch).

The peak associated with O—H bond at 3263 cm^{-1} in native starch was shifted to 3270 cm^{-1} in LBS and 3282 cm^{-1} in NABS and LABS. The predominant peak shift for O—H group in NABS and LABS indicates that autoclaved-retrogradation treatment increased the crystalline region, leading to the structural alterations [30]. The bond (C—H) allocated at 2927 cm^{-1} in native starch was found at the same position in LBS but shifted to 2923 and 2924 cm^{-1} in NABS and LABS respectively. Another major shift in wavelength was observed for the bond associated with C═O, C—C—C, and C—C—H functional groups and shift occurred from 1337 to 1338 cm^{-1} (NBS and LBS) to 1360–1361 cm^{-1} (NABS and LABS). There was no major difference in intensity and shape of peaks between NBS and LBS but the peaks were observed to shift greatly after heat treatment (NABS and LABS). This indicated the modification in specific starch structures and bonding after acid hydrolysis and autoclaving-retrogradation treatments [11].

3.3. Swelling power and solubility of culled banana resistant starch

Fig. 3 illustrates the swelling power and solubility of culled banana resistant starch samples. NBS showed significantly higher ($p < 0.05$)

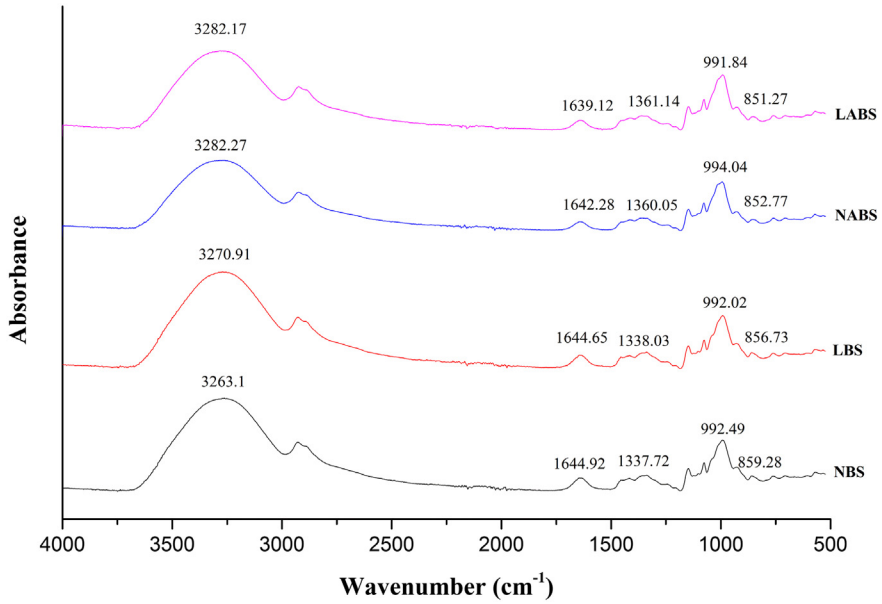

Fig. 2. FTIR spectra of NBS (native banana starch), LBS (lintnerized banana starch), NABS (native-autoclaved banana starch) and LABS (lintnerized-autoclaved banana starch).

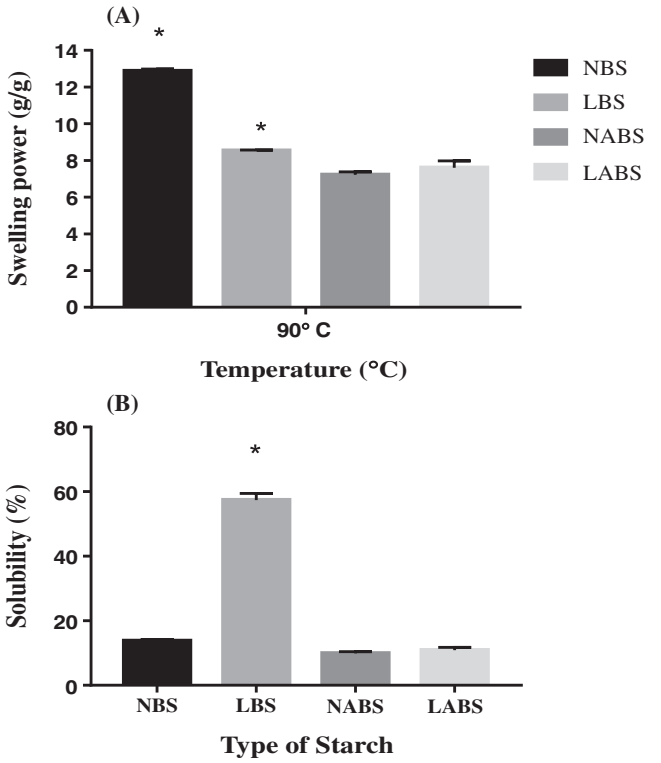

Fig. 3. Swelling power (A) and water solubility (B) of NBS (native banana starch), LBS (lintnerized banana starch), NABS (native-autoclaved banana starch) and LABS (lintnerized-autoclaved banana starch). Significant ($p < 0.05$) differences between groups are indicated by *.

swelling power (12.87 g/g) whereas, after acid hydrolysis the value was decreased to 8.53 (g/g) in LBS. There was no significant ($p < 0.05$) difference in swelling power of heat-treated starches *i.e.* NABS (7.22 g/g) and LABS (7.60 g/g). Swelling power of the starch refers to hydration capacity resulting from interaction between crystalline and amorphous structure within the starch granules. The destruction of starch granule during acid-hydrolysis, gelatinization and retrogradation process lowers the swelling power of LBS, NABS and LABS [10].

The solubility of NBS (13.78%) increased significantly ($p < 0.05$) after acid-hydrolysis and found 57.3% in LBS (Fig. 3B). The increased solubility of LBS might be due to starch chain depolymerization induced by acid hydrolysis [27]. NABS (9.92%) and LABS (10.9%) exhibited solubility significantly ($p < 0.05$) lower than the LBS. The solubility values are related to granular structure, molecular weight, formation of short chain hydroxyl group and increase in amylose content [31]. The autoclaved starch samples showed lower solubility than corresponding raw materials (native and lintnerized starch). This can be explained by the fact that autoclaved starch samples (NABS and LABS) exhibited higher amylose content that was accountable for decreased solubility.

3.4. Conjugation of resistant starch-soy protein isolate

Based on chemical composition, characterization and functional properties, LABS was selected to conjugate with soy protein. Proteins and polysaccharides conjugated by covalent linkage or Maillard reaction shows synergistic effects on emulsion stability [32].

Different combinations of LABS and SPI (1:1, 2:1 and 2:3, w/w) were selected for conjugation. The conjugates were further characterized by FTIR chemical finger-printing to observe the covalent bonding in conjugates formed during Maillard reaction (Fig. 4). Chemical finger printing of SPI showed dominant absorption peaks at 1627 cm^{-1}, 1515.73 cm^{-1}, 1394 cm^{-1} and 1234 cm^{-1} which attributed to C═O stretching for amide I, N—H bending vibration for amide II and C—N stretching and N—H bending of amide III respectively [33,34]. For LABS dominant absorption peaks were observed at 3282 cm^{-1} (O—H stretching), 2924.58 cm^{-1} (C—H stretching), 1147 cm^{-1} (C—H vibration), 1077 cm^{-1}(C—O stretching), 991 cm^{-1} (crystallinity structure) [11].

In LABS-SPI conjugates, O—H stretching vibration (3297–3316 cm^{-1}), C—H stretching vibration (peak around 2930 cm^{-1}) were found intensified compared to FTIR spectra of SPI and LABS. Formation of new peaks in LABS-SPI conjugates were observed at 1545 cm^{-1} and 1155 cm^{-1} corresponded to C═O stretching and C—N stretching respectively. Moreover, the absorption band at amide region (1630–1650 cm^{-1}) was intensified and a new peak was observed at 1660 cm^{-1} which presented stretching of Schiff's base

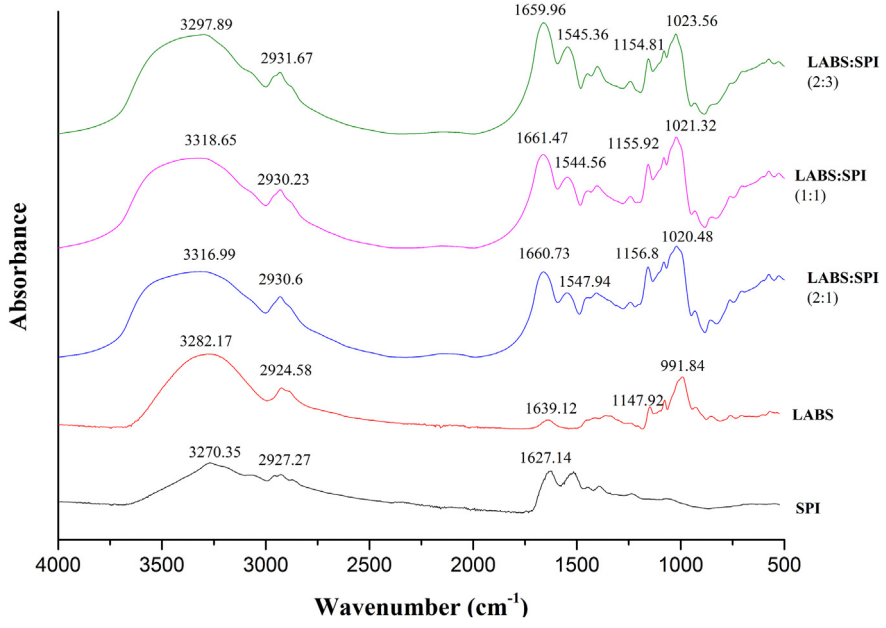

Fig. 4. FTIR spectra of SPI (soy protein isolate), LABS (lintnerizaed autoclaved banana starch) and LABS-SPI conjugates.

Table 2
Emulsion stability and creaming index of the emulsions.

Emulsion system (LABS: SPI)	Emulsion stability (%)	Creaming index (%)
E_1 (0:1)	93.62 ± 4.75^{ab}	12.19 ± 2.44^{ac}
E_2 (1:1)	106.22 ± 1.65^{bc}	5.4 ± 1.22^{b}
E_3 (2:1)	109.06 ± 2.17^{bc}	6.12 ± 2.12^{bc}
E_4 (2:3)	127.32 ± 11.66^{c}	4.67 ± 1.17^{b}
E_5 (0:1)	77.33 ± 2.52^{a}	16.67 ± 2.31^{d}
E_6 (1:1)	123.99 ± 6.38^{c}	11.26 ± 0.75^{ac}
E_7 (2:1)	82.29 ± 6.85^{ab}	16.76 ± 2.64^{d}
E_8 (2:3)	91.92 ± 8.82^{ab}	11.25 ± 1.29^{ac}

E_1 = 10% SPI + 5% oil: E_2 = 5% LABS +5% SPI + 5% oil; E_3 = 6.67% LABS +3.33% SPI + 5% oil; E_4 = 4% LABS +6% SPI + 5% oil; E_5 = 5% SPI + 10% oil; E_6 = 2.5% LABS +2.5% SPI + 10% oil; E_7 = 3.33% LABS +1.67% SPI + 10% oil; E_8 = 2% LABS +3% SPI + 10% oil.
Different superscript letters (a-d) indicate significant ($p < 0.05$) difference among mean observations.

imine group and enaminol group resulting from covalent bonds formation between amide group and carbonyl group during Maillard reaction [33].

3.5. Emulsion stability and creaming index

LABS-SPI conjugates (1:1, 2:1, 2:3 w/w) and sunflower oil (5 and 10%) were used to formulate oil-in-water emulsions (Table 2). Emulsions were stored at 4 °C and observed for cream layer separation for the period of 14 days. At the end of the storage period, the highest layer of the cream separation was observed in the emulsions made of soy protein isolate alone while the emulsion prepared from resistant starch-protein conjugate showed better creaming stability.

The emulsions prepared using SPI as the sole emulsifier exhibited lower emulsion stability, which indicated that alone SPI was not an ideal emulsifier. Similar results were reported earlier for egg-shell membrane protein hydrolysates [4] and rice dreg protein hydrolysates [19] indicating that only proteins were not able to form stable emulsion due to coalescence. The emulsion stability was found to increase with the addition of LABS-SPI conjugates as the *co*-existence of both polysaccharides and protein resulted in the formation of thick and compact layers that cover the oil droplets resulting in steric stabilization [4]. The optimum ratio for emulsion stability depends on the types of proteins and polysaccharides utilized. Kasran et al. [7] reported that soy whey protein isolate: fenugreek gum conjugates at ratios 1: 3 and 1: 5

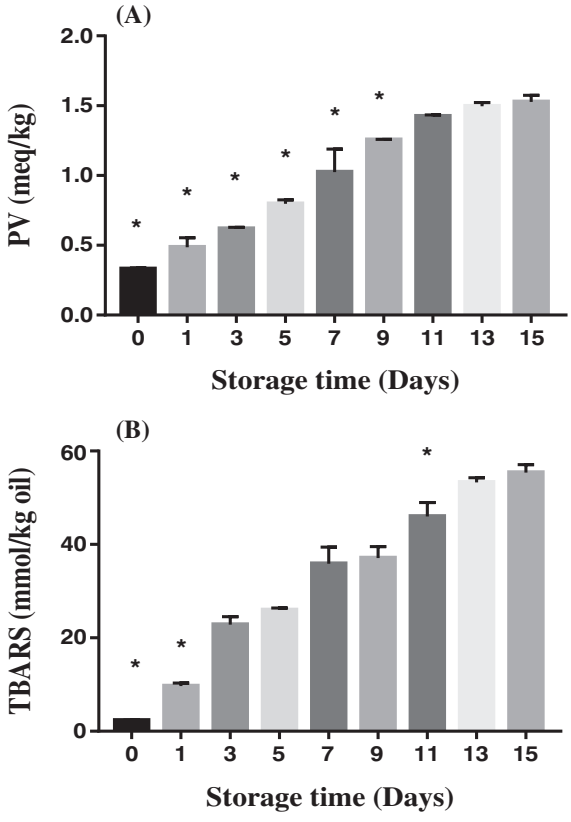

Fig. 5. PV and TBARS value of emulsions stored at 25 °C. Significant ($p < 0.05$) differences between groups are indicated by *.

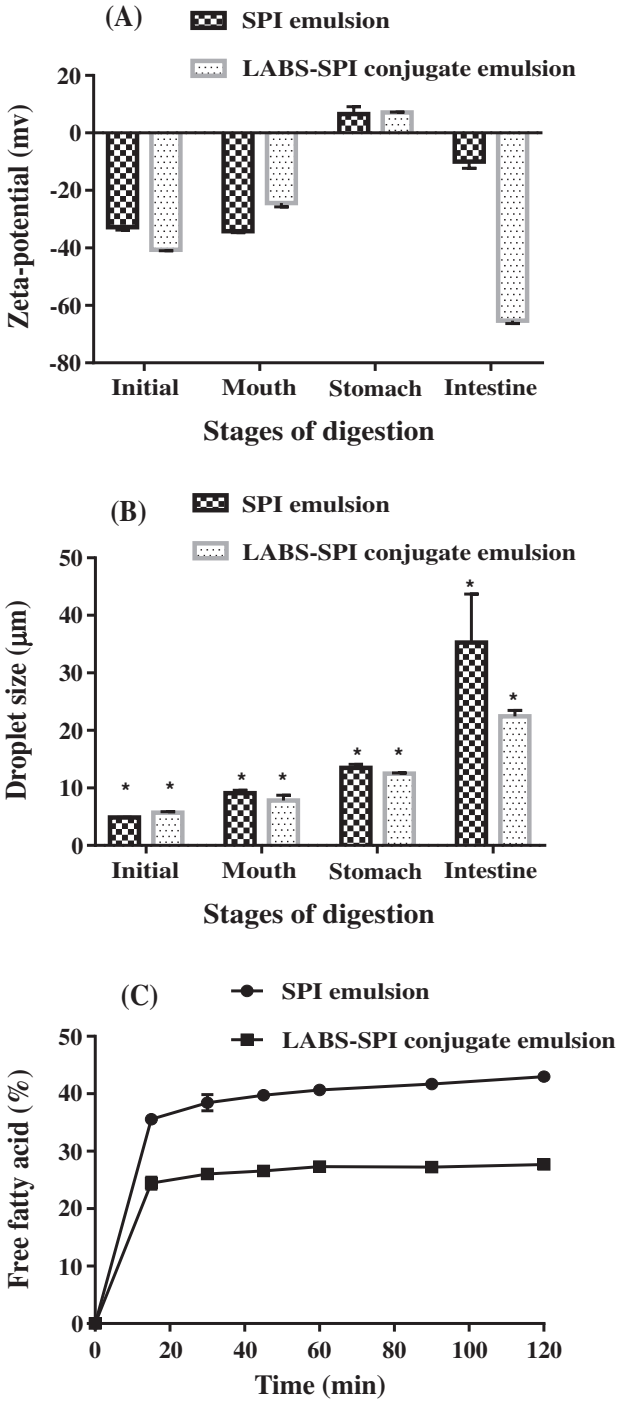

Fig. 6. Changes in droplet properties: zeta potential (A); droplet size (B) throughout the *in vitro* digestion model; and free fatty acids (FFA %) released in the intestine phase (C) of the emulsions stabilized by SPI and LABS-SPI conjugate. Significant ($p < 0.05$) differences between mean observations are indicated by *.

were more effective compared to 1:1 ratio (w/w) in stabilizing the emulsion.

3.6. Characterization of LABS-SPI conjugate based emulsion

The emulsion prepared by using LABS-SPI conjugate (2:3) as wall material (10%) and sunflower oil (5%) as the oil phase was found most stable emulsion system (Table 2) and further characterized for oxidative stability and *in vitro* digestion behavior.

3.6.1. Oxidative stability of emulsion

Fig. 5 illustrates the oxidative stability of emulsion, which was evaluated during the storage of emulsion at 25 °C, for 15 days. PV of the emulsion was gradually increased from 0.33 to 1.514 meq/kg oil during the 15 days of storage. Nasrin and Anal [11] reported lower PV in emulsion system made by culled banana RS-SPI conjugate compared to SPI emulsion, which indicated the ability of RS-SPI conjugate to prevent the lipid oxidation.

TBARS value of the emulsion increased progressively from 3.99 to 56.33 μmol/kg during 15 days of storage. The formation of primary and secondary products of lipid oxidation is associated with the processing condition, such as high-pressure homogenization reduces the droplet size which in turn increases the surface area per unit volume of the droplets to pro-oxidant at the interface and storage temperature [35].

3.6.2. In-vitro digestion of emulsion

3.6.2.1. Zeta potential. Zeta potential characterizes the changes in the emulsion electrical properties, which indirectly measures the change in interfacial composition of the emulsion droplets as it progresses through different stages of the *in vitro* digestion system. Kim et al. [36] reported that the colloidal system with higher zeta potential (≥ ± 40 mV) are predicted to be electrically stable. A higher value of zeta potential indicates the presence of higher electrostatic repulsion and larger distances between the droplets that results in lesser flocculation and aggregation. Zeta potential of the LABS-SPI stabilized emulsion (−40.63 mV) was significantly ($p < 0.05$) higher than control SPI stabilized emulsion (−32.83 mV). The higher electrostatic repulsion in LABS-SPI stabilized emulsion indicated lower inter-droplet attraction, droplet flocculation, aggregation and better emulsion stability. When the emulsions were incubated with simulated saliva, the magnitude of zeta potential changed but the charged remained anionic.

As the emulsion passed from mouth to simulated gastric phase, the magnitude of the zeta potential change appreciably and exhibited cationic charge. The positive charge was likely due to the fact that the pH of simulated gastric fluid was less than the pI of SPI. The observed changes in the zeta potential of both emulsions (SPI stabilized and LABS-SPI stabilized emulsions) could be attributed to changes in pH, which could increase the positive charge of SPI, or displacement of original emulsifier caused by digestion of WPI by pepsin [37]. Finally, when

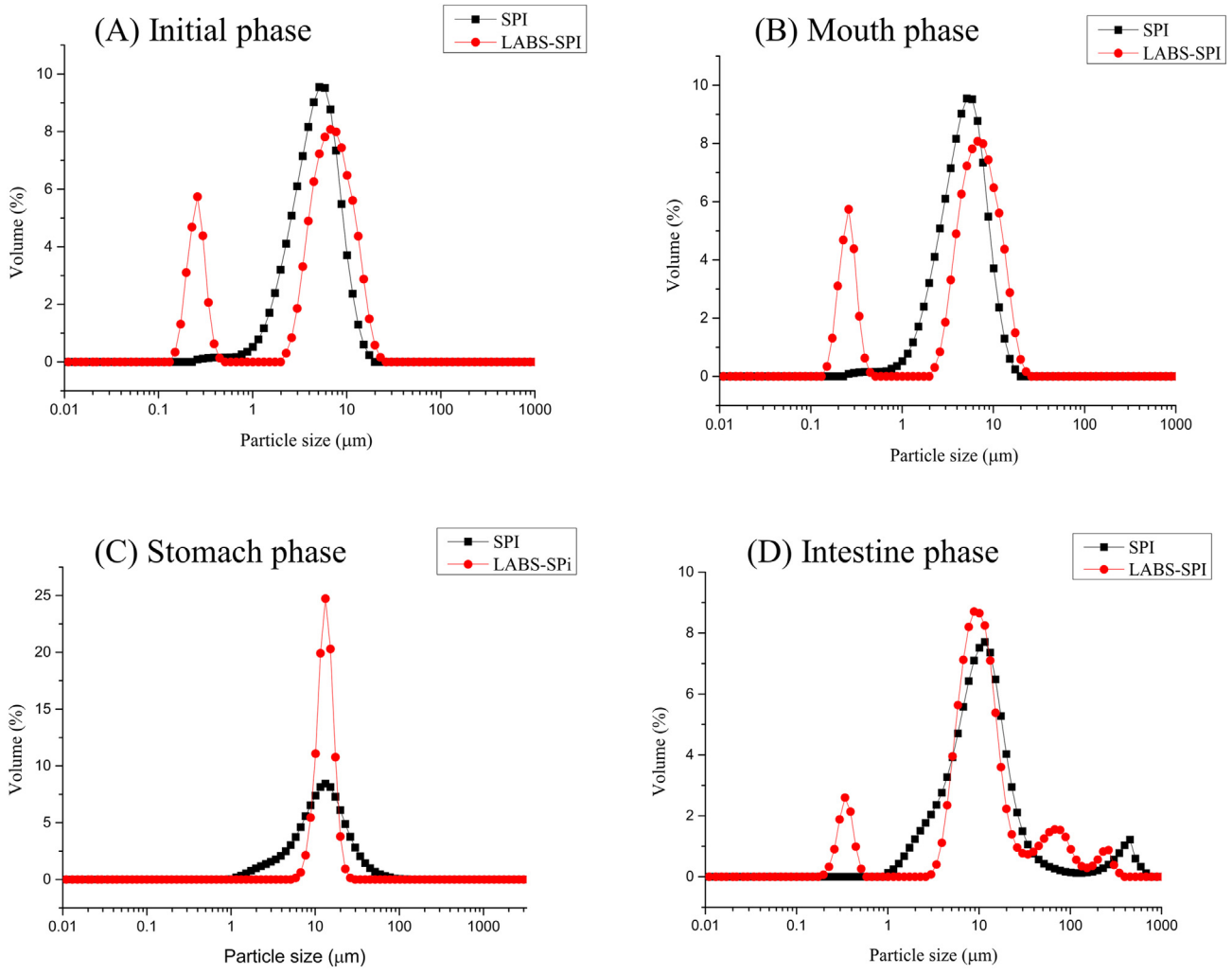

Fig. 7. Droplet size distribution of the emulsions stabilized by SPI and LABS-SPI conjugate during passage through *in vitro* digestion model: (A) Initial phase; (B) Mouth phase: (C) Stomach phase; and (D) Intestine phase.

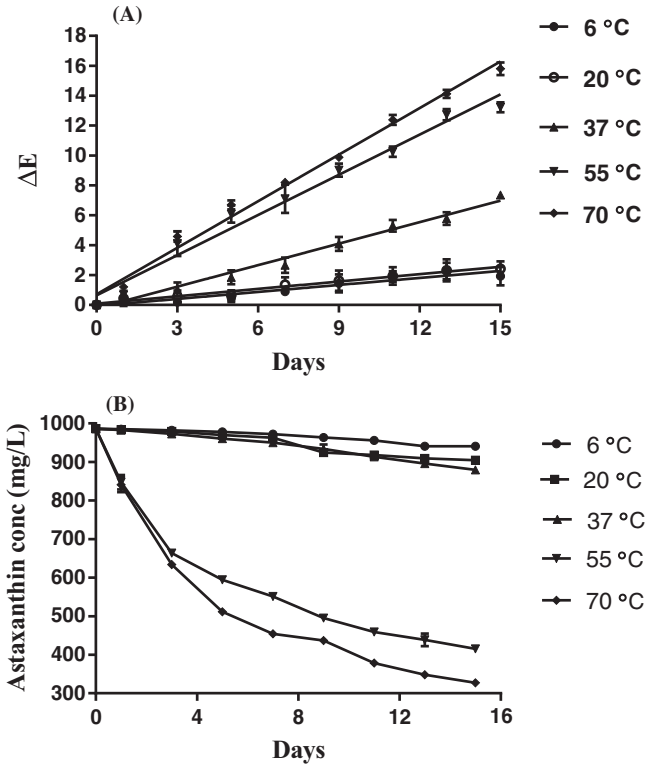

Fig. 8. Total color difference of astaxanthin enriched emulsion (ΔE) (A) and change in astaxanthin concentration at different storage temperatures (B).

emulsion was incubated with SIF the droplets became negatively charged for both SPI stabilized emulsion (−10.00 ± 2.25 mV) and LABS-SPI stabilized emulsion (−65.33 ± 0.99 mV) (Fig. 6A). However, the droplet charge in emulsion stabilized by LABS-SPI conjugate was more negative than the SPI stabilized emulsion. The high negative charge of the LABS-SPI stabilized emulsion was due to the adsorption of resistant starch on the surface of protein-coated droplets that in turn decreased the protein displacement [38].

3.6.2.2. Droplet size and particle size distribution. Droplet size and particle size distribution of the emulsion systems were determined by using the laser light scattering techniques as they passed through each phase of *in vitro* digestion model (Figs. 6B and 7). The initial emulsion system stabilized by SPI, exhibited monomodal size distribution while the LABS-SPI stabilized emulsion showed additional small droplet peak (0.1–1 μm) (Fig. 7A). The initial mean droplet diameters of the SPI and LABS-SPI conjugate stabilized emulsions were similar *i.e.* 4.84 μm and 5.69 μm respectively. This indicates that presence of resistant starch (LABS) did not promote droplet aggregation and both SPI alone and LABS-SPI conjugates were capable of stabilizing the emulsion system.

When the emulsions were passed through the simulated mouth model, there was no significant change in the mean droplet sizes and particle size distribution (Fig. 7B). This might be due to insignificant amount of surface active components to displace the emulsifiers. Similar to this result no significant change in mean droplet diameter and particle size distribution was reported in the gastric phase of the emulsion stabilized by whey protein isolate (WPI) and beet pectin (BP) [37]. When the emulsion from mouth phase was passed through simulated gastric phase, the increase in the droplet size was observed and the monomodal particle size distribution appeared (Fig. 7C) for both the emulsions with disappearance of smaller droplet peak. The change in droplet size distribution of the SPI and LABS-SPI conjugate stabilized emulsions might be due to the action of pepsin that digested and displaced the adsorbed protein layer. The interaction of simulated stomach components with the surface of the droplets in emulsions are reported to change droplet size distribution [37].

Finally, the emulsion from gastric phase was passed through simulated intestinal phase. After incubation in simulated intestinal phase the particle size distribution and droplet size increased significantly, the droplet size of SPI stabilized emulsion (31 μm) was significantly greater than droplet size of LABS-SPI stabilized emulsion (22 μm), which suggested that the LABS-SPI conjugate was more effective at protecting the stability of the emulsion to droplet destabilization during digestion. The emulsion systems showed loss of small droplets meanwhile larger droplet size peak appeared in the particle size distribution (Fig. 7D). This higher increase in droplet size of SPI stabilized emulsion indicated that presence of resistant starch had an influence on the droplet digestion process, possibly by altering the droplet coalescence or by hindering the ability of digestive enzymes to adsorb to the droplet surfaces.

3.6.2.3. Free fatty acid release. The amount of FFA released in emulsion stabilized by SPI (42.97 ± 0.51%) alone was found higher than that stabilized by conjugate of LABS-SPI (27.67 ± 0.27%) (Fig. 6C). This can be best exemplified by the fact that conjugates retard the FFA release by forming protecting interfacial layer which in turn reduced the action of the enzymes on the lipids [37]. The amount of free fatty acids released helps to determine the rate and magnitude of lipid digestion in the intestine. The result shows that there was a huge surge in the quantity of free fatty generated during the first 20 min which then further gradually increased throughout the digestion process.

3.7. Thermal stability of the astaxanthin enriched emulsion

The astaxanthin enriched emulsions were incubated at different temperature (6, 20, 37, 55 and 70 °C) for 15 days. The changes in the color of emulsion were evaluated by monitoring the changes in color parameters (CIE L*a* b* system). Increase in lightness (L*-value), decrease in redness (a*) and yellowness (b*) were observed in the emulsion during the total storage period (Supplementary Fig. S1). The total color difference (ΔE) of emulsions was calculated at variable temperature range (Fig. 8A) and the color degradation rate was calculated as the slope of the linear regression of ΔE *vs* time. The color change rate was found to be strongly dependent on the storage temperature *i.e.* higher the surrounding temperature larger the color degradation rate. There was no significant difference in the color degradation rate of the

Table 3
Astaxanthin degradation rate constant at different storage temperatures.

Storage temperature (°C)	First-order degradation	$k \times 10^{-2}$ (day^{-1})	R^2	Activation energy KJ mol^{-1}
6	C = 986.49 [−exp (0.00343) t]	0.34[a]	0.95	39.909
20	C = 986.49 [−exp (0.00643) t]	0.64[b]	0.95	
37	C = 986.49 [−exp (0.00763) t]	0.76[b]	0.94	
55	C = 986.49 [−exp (0.05417) t]	5.42[c]	0.92	
70	C = 986.49 [−exp (0.07043) t]	7.04[d]	0.93	

k = degradation rate constant, R2 = square of correlation coefficient, C = astaxanthin concentration.
Different superscript letters (a-d) indicate significant ($p < 0.05$) difference among the observations.

emulsions stored at 6 °C (0.16 day^{-1}) and 20 °C (0.17 day^{-1}) but it was found to increase significantly with increase in incubation temperature with the highest color degradation at 70 °C (1.04 day^{-1}). The activation energy for color degradation (27 KJ mol^{-1}) was found to be higher than previously reported by Liu et al. [22] for astaxanthin enriched sodium caseinate emulsion (15.2 KJ mol^{-1}) but lower than lutein enriched emulsion activation energy (37.98 KJ mol^{-1}) as reported by Davidov-Pardo et al. [21].

Due to unsaturated structure, astaxanthin is sensitive to heat, light and oxygen and therefore, tends to degrade during storage [35]. Thermal stability of astaxanthin was monitored based on the amount of astaxanthin retained in emulsion during storage at different temperatures (6, 20, 37, 55 and 70 °C) (Fig. 8B). Astaxanthin concentration in the emulsion decreased with increase in storage time and temperature. After storage at 6, 20, 37, 55 and 70 °C for 15 days, the initial astaxanthin concentration (987 mg/L) decreased to 940, 905, 876, 415 and 327 mg/L respectively which indicated that astaxanthin degraded faster at higher temperature than that at lower temperature.

Astaxanthin concentration degradation was analyzed by first order reaction kinetics as reported by previous research studies [16,39,40]. Table 3 shows the degradation rate constant (day^{-1}) at different temperatures and activation energy. The degradation rate constant was found to increase with the increase in temperature. There was no significant difference between k values of emulsions stored at 20 and 37 °C while, degradation rate constant was significantly higher in emulsions stored at 55 and 70 °C. The activation energy was 40 KJ mol^{-1} which was higher than color degradation activation energy.

4. Conclusion

Resistant starch was isolated from culled banana pulp, converted to RS III and characterized. Lintnerized-autoclaved banana starch exhibited the better functional properties and conjugated with SPI. Chemical finger printing of the conjugate showed the formation of Maillard reaction products. The emulsion prepared by utilizing the resistant starch-SPI conjugate as wall material showed physical and electrical stability compared to the emulsion prepared by SPI only. Resistant starch-SPI conjugate based emulsion systems with better stability can be used to fortify and deliver various bioactive compounds in functional food systems, nutraceutical and cosmetic products.

Supplementary data to this article can be found online at https://doi.org/10.1016/j.ijbiomac.2018.08.066.

Conflict of interest statement

The authors declare no conflict of interest.

Acknowledgement

The authors acknowledge Royal Thailand Government (RTG) for providing Her Majesty the Queen's Scholarship to one of the author to conduct this research project.

References

[1] A. Marefati, M. Bertrand, M. Sjöö, P. Dejmek, M. Rayner, Storage and digestion stability of encapsulated curcumin in emulsions based on starch granule Pickering stabilization, Food Hydrocoll. 63 (2017) 309–320.
[2] W. Lu, A.L. Kelly, S. Miao, Emulsion-based encapsulation and delivery systems for polyphenols, Trends Food Sci. Technol. 47 (2016) 1–9.
[3] D.J. Mcclements, Critical review of techniques and methodologies for characterization of emulsion stability, Crit. Rev. Food Sci. Nutr. 47 (2007) 611–649.
[4] S. Jain, A.K. Anal, Preparation of eggshell membrane protein hydrolysates and culled banana resistant starch-based emulsions and evaluation of their stability and behavior in simulated gastrointestinal fluids, Food Res. Int. 103 (2018) 234–242.
[5] M. Evans, I. Ratcliffe, P.A. Williams, Emulsion stabilisation using polysaccharide–protein complexes, Curr. Opin. Colloid Interface Sci. 18 (2013) 272–282.
[6] M. Akhtar, R. Ding, Covalently cross-linked proteins & polysaccharides: formation, characterization and potential applications, Curr. Opin. Colloid Interface Sci. 28 (2017) 31–36.
[7] M. Kasran, S.W. Cui, H.D. Goff, Covalent attachment of fenugreek gum to soy whey protein isolate through natural Maillard reaction for improved emulsion stability, Food Hydrocoll. 30 (2013) 552–558.
[8] J. Wang, X.J. Tang, P.S. Chen, H.H. Huang, Changes in resistant starch from two banana cultivars during postharvest storage, Food Chem. 156 (2014) 319–325.
[9] P. Zhang, R.L. Whistler, J.N. Bemiller, B.R. Hamaker, Banana starch: production, physicochemical properties, and digestibility—a review, Carbohydr. Polym. 59 (2005) 443–458.
[10] C.K. Reddy, M. Suriya, P.V. Vidya, S. Haripriya, Synthesis and physico-chemical characterization of modified starches from banana (Musa AAB) and its biological activities in diabetic rats, Int. J. Biol. Macromol. 94 (2017) 500–507.
[11] T.A.A. Nasrin, A.K. Anal, Resistant starch III from culled banana and its functional properties in fish oil emulsion, Food Hydrocoll. 35 (2014) 403–409.
[12] C. Chung, L. Sanguansri, M.A. Augustin, Resistant starch modification: effects on starch properties and functionality as co-encapsulant in sodium caseinate-based fish oil microcapsules, J. Food Sci. 75 (2010) 636–642.
[13] I. Higuera-Ciapara, L. Felix-Valenzuela, F.M. Goycoolea, Astaxanthin: a review of its chemistry and applications, Crit. Rev. Food Sci. Nutr. 46 (2006) 185–196.
[14] M.W. Dethlefsen, N.H. Hjermitslev, S. Frosch, M.E. Nielsen, Effect of storage on oxidative quality and stability of extruded astaxanthin-coated fish feed pellets, Anim. Feed Sci. Technol. 221 (2016) 157–166.
[15] A.A. Martínez-Delgado, S. Khandual, S.J. Villanueva-Rodríguez, Chemical stability of astaxanthin integrated into a food matrix: effects of food processing and methods for preservation, Food Chem. 225 (2017) 23–30.
[16] A. Bustamante, L. Masson, J. Velasco, J.M. del Valle, P. Robert, Microencapsulation of *H. pluvialis* oleoresins with different fatty acid composition: kinetic stability of astaxanthin and alpha-tocopherol, Food Chem. 190 (2016) 1013–1021.
[17] F. Tamjidi, M. Shahedi, J. Varshosaz, A. Nasirpour, Design and characterization of astaxanthin-loaded nanostructured lipid carriers, Innovative Food Sci. Emerg. Technol. 26 (2014) 366–374.
[18] S.O. Serna-Saldivar, Cereal Grains: Laboratory Reference and Procedures Manual, CRC Press, Boca Raton, FL, USA, 2012 (Chapter 2).
[19] Q. Zhao, C. Selomulya, S. Wang, H. Xiong, X.D. Chen, W. Li, H. Peng, J. Xie, W. Sun, Q. Zhou, Enhancing the oxidative stability of food emulsions with rice dreg protein hydrolysate, Food Res. Int. 48 (2012) 876–884.
[20] K.R. Kuhn, R.L. Cunha, Flaxseed oil–whey protein isolate emulsions: effect of high pressure homogenization, J. Food Eng. 111 (2012) 449–457.
[21] G. Davidov-Pardo, C.E. Gumus, D.J. McClements, Lutein-enriched emulsion-based delivery systems: influence of pH and temperature on physical and chemical stability, Food Chem. 196 (2016) 821–827.
[22] X. Liu, D.J. McClements, Y. Cao, H. Xiao, Chemical and physical stability of astaxanthin-enriched emulsion-based delivery systems, Food Biophys. 11 (2016) 302–310.
[23] C. Niamnuy, S. Devahastin, S. Soponronnarit, G.V. Raghavan, Kinetics of astaxanthin degradation and color changes of dried shrimp during storage, J. Food Eng. 87 (2008) 591–600.
[24] B.A. Ashwar, A. Gani, I.A. Wani, A. Shah, F.A. Masoodi, D.C. Saxena, Production of resistant starch from rice by dual autoclaving-retrogradation treatment: invitro digestibility, thermal and structural characterization, Food Hydrocoll. 56 (2016) 108–117.
[25] L.F. Polesi, S.B.S. Sarmento, Structural and physicochemical characterization of RS prepared using hydrolysis and heat treatments of chickpea starch, Starch-Starke 63 (2011) 226–235.
[26] R.G. Utrilla-Coello, M.E. Rodríguez-Huezo, H. Carrillo-Navas, C. Hernández-Jaimes, E.J. Vernon-Carter, J. Alvarez-Ramirez, In vitro digestibility, physicochemical, thermal and rheological properties of banana starches, Carbohydr. Polym. 101 (2014) 154–162.
[27] A. Aparicio-Saguilán, E. Flores-Huicochea, J. Tovar, F. García-Suárez, F. Gutiérrez-Meraz, L.A. Bello-Pérez, Resistant starch-rich powders prepared by autoclaving of native and lintnerized banana starch: partial characterization, Starch-Starke 57 (2005) 405–412.
[28] P. Nimsung, M. Thongngam, O. Naivikul, Compositions, morphological and thermal properties of green banana flour and starch, Kasetsart J. (Nat. Sci.) 41 (2007) 324–330.
[29] T.A.A. Nasrin, A. Noomhorm, A.K. Anal, Physico-chemical characterization of culled plantain pulp starch, peel starch, and flour, Int. J. Food Prop. 18 (2015) 165–177.
[30] M. García-Rosas, A. Bello-Pérez, H. Yee-Madeira, G. Ramos, A. Flores-Morales, R. Mora-Escobedo, Resistant starch content and structural changes in maize (*Zea mays*) tortillas during storage, Starch-Starke 61 (2009) 414–421.
[31] C.K. Reddy, S. Pramila, S. Haripriya, Pasting, textural and thermal properties of resistant starch prepared from potato (Solanum tuberosum) starch using pullulanase enzyme, J. Food Sci. Technol. 52 (2015) 1594–1601.
[32] H. Koksel, T. Masatcioglu, K. Kahraman, S. Ozturk, A. Basman, Improving effect of lyophilization on functional properties of resistant starch preparations formed by acid hydrolysis and heat treatment, J. Cereal Sci. 47 (2008) 275–282.
[33] Y. Yang, S.W. Cui, J. Gong, Q. Guo, Q. Wang, Y. Hua, A soy protein-polysaccharides Maillard reaction product enhanced the physical stability of oil-in-water emulsions containing citral, Food Hydrocoll. 48 (2015) 155–164.
[34] L. Wang, M. Wu, H.M. Liu, Emulsifying and physicochemical properties of soy hull hemicelluloses-soy protein isolate conjugates, Carbohydr. Polym. 163 (2017) 181–190.

[35] J. Pu, J.D. Bankston, S. Sathivel, Developing microencapsulated flaxseed oil containing shrimp (*Litopenaeus setiferus*) astaxanthin using a pilot scale spray dryer, Biosyst. Eng. 108 (2011) 121–132.
[36] D.M. Kim, S.S. Hyun, P. Yun, C.H. Lee, S.Y. Byun, Identification of an emulsifier and conditions for preparing stable nanoemulsions containing the antioxidant astaxanthin, Int. J. Cosmet. Sci. 34 (2012) 64–73.
[37] D. Xu, F. Yuan, Y. Gao, A. Panya, D.J. McClements, E.A. Decker, Influence of whey protein–beet pectin conjugate on the properties and digestibility of β-carotene emulsion during *in vitro* digestion, Food Chem. 156 (2014) 374–379.
[38] S.J. Hur, E.A. Decker, D.J. McClements, Influence of initial emulsifier type on microstructural changes occurring in emulsified lipids during *in vitro* digestion, Food Chem. 114 (2009) 253–262.
[39] C. Bustos-Garza, J. Yáñez-Fernández, B.E. Barragán-Huerta, Thermal and pH stability of spray-dried encapsulated astaxanthin oleoresin from *Haematococcus pluvialis* using several encapsulation wall materials, Food Res. Int. 54 (2013) 641–649.
[40] M. Vakarelova, F. Zanoni, P. Lardo, G. Rossin, F. Mainente, R. Chignola, A. Menin, C. Rizzi, G. Zoccatelli, Production of stable food-grade microencapsulated astaxanthin by vibrating nozzle technology, Food Chem. 221 (2017) 289–295.